J Mater Sci (2008) 43:1559–1567
DOI 10.1007/s10853-007-2339-6

Study on microstructure and properties of Ni-based alloy/Y_2O_3-deposited metals by laser cladding

Pei Quan Xu · Hong Ying Gong · Guo Xiang Xu · Jian Ping He · Zhi Shui Yu

Received: 2 May 2007 / Accepted: 21 November 2007 / Published online: 31 December 2007

Abstract Laser cladding of Ni-based alloy/Y_2O_3 (Yttrium Oxide) powder on 6061 aluminum alloy was carried out using 3 kW CW Nd:YAG laser to strengthen and improve hardness and corrosion resistance of substrate. Metal matrix composite composed of aluminum substrate, Ni-based alloy, refining and dispersion strengthening Y_2O_3, and particle hardening W, Cr was obtained. The microstructure and morphology, phase identification, element diffusion, and composition analysis of the Ni-based alloy/Y_2O_3-deposited metal and deposited metals/6061 aluminum substrate interface were examined using scanning electron microscopy (SEM), Electron Probe Micro-analyzer (EPMA) with energy-dispersive spectrometer (EDS) analysis. The microhardness distribution and corrosion-resistance property were investigated also. The results showed: (1) with the addition of Y_2O_3, more fine microstructures consisted of isometric crystal, white acicular crystal, and fringe crystal, primary phases were mainly Ni_3Al, NiAl, $NiAl_3$, W, α-Al, and Cr_xC. (2) Micro-hardness of deposited metals was 780–1100 $HV_{0.2}$ and distributed smoothly near interface. The corrosion rate of aluminum substrate was nearly twice that of deposited metals with addition of Y_2O_3.

Introduction

Strengthening phase structures are often introduced into alloys for surface modification purposes by different surface modification techniques. An obvious example is the extremely fine second-phase particles used for precipitation and dispersion hardening [1]. Generally speaking, surface modification techniques include plating techniques (electrocladding, chemical plating, ion plating, and magnetron sputtering), ion implantation and deposition, spraying techniques (flame spraying, plasma spraying, and electric arc spraying) etc. However, while using plating technique, it is easy to flake off for coating from substrate in special chemical mediator because of two-dimensional materials structure and weak bonding with chemical or mechanical force between coating and substrate.

While using spraying technique, thicker coating could be obtained, but the bonding between coating and substrate belongs to mechanical joining with weakness and such drawbacks as gas porosity. Therefore, it is of interest to develop a surface modification technique, e.g., by laser cladding with a new material-deposited metal system design that provides good combination of desirable mechanical properties, in particular, both high strength and good corrosion-resistance properties. Rapid materials processing, such as laser cladding technique, is steadily becoming a tool for synthesis of materials, as well as rapid manufacturing. Recently, a large number of new clad materials and composites have been developed. Clad material included ceramic phases, strengthening wearing phases, or special crystalline materials, e.g. Al_2O_3, NiTi [2–6], in situ synthesis TiC coating [7, 8], WC/Ni coating [9, 10], quasicrystal, and amorphous mixtures [11–20], in which the hardening phase itself has a coarse scale structure. While such materials offer high strength, they usually have to suffer from porosity and contamination problems in laser cladding process.

In this article, we discuss the microstructure and mechanical properties of Ni-based/Y_2O_3-deposited metal (different ratio of Y_2O_3) on 6061 Al alloys. In Section "Microstructure design strategy", we first present a general

P. Q. Xu (✉) · H. Y. Gong · G. X. Xu · J. P. He · Z. S. Yu
College of Materials Engineering, Shanghai University of Engineering Science, Shanghai 201620, China
e-mail: xupeiquan7810@yahoo.com.cn

discussion of the microstructure design strategy. The experimental procedures are described in Section "Experimental". Section "Results" demonstrates the microstructure, composition analysis, and desirable mechanical properties of the alloys, including its high micro-hardness in combination with corrosion resistance, and in particular its strong fine-particle hardening ability. To correlate the properties with microstructure, a detailed structural and compositional analysis of the microstructures before and after addition of Y_2O_3 is given in Section "Results". Section "Discussions" dicussess the dislocation slip characteristics uncovered in microscopy studies are used to explain the strength, particle hardening, and grain refinement observed. Section "Conclusion" highlights the benefits that can be derived from addition of Y_2O_3.

Microstructure design strategy

To achieve high-strength clad layers with high-corrosion resistance property, we desire a Ni-based alloys/Y_2O_3-deposited metal structure that can be obtained on the surface of aluminum alloys by using laser cladding technique, properly choosing the deposited metals composition and controlling the laser cladding parameters. It is important to note that together with the fine microstructure, a corrosion-resistant phase with a much larger grain size can be designed to be among the solidification phases. We select Ni-based alloy composition of $Ni_{48}Cr_{14}Co_8CMo_5W_{12}Al_6Fe_6$, wherein, elements such as Cr and W show high-strength property; and elements such as Ni, Co, Fe play two key roles for the clad layer: one is well-binding phase between deposited metal and aluminum substrate, the other is good-resistant material from reactive phases (Ni_xAl, Fe_xAl, etc.). To obtain the fine microstructure, deposited metals are ranged from different ratio of Ni-based alloys and Y_2O_3 addition (0, 2, 6, and 8%, respectively), and as such the solidification products will produce the desired microstructure as discussed in the preceding paragraph. The multiple elements addition also renders the crystal growth more sluggish, favoring the refinement of coarse scales to fine scales.

Experimental

6061 Aluminum alloys (Al–Mg–Si) are selected as base materials, the details are: dimension: 60 × 50 × 30 mm; surface roughness: 0.2 μm; and its chemical composition is given in Table 1. The deposited alloys are mixture of Ni-based alloys and Rare earth oxide (Yttrium Oxide) after milling. Molecular formula: Y_2O_3; Molecular weight: 225.82; Technical condition: $Y_2O_3 \geq 99.99\%$; $CeO_2 \leq 0.0005\%$; $Pr_6O_{11} \leq 0.0005\%$; $Nd_2O_3 \leq 0.0005\%$; $Sm_2O_3 \leq 0.0005\%$; $La_2O_3 \leq 0.0005\%$; $Ho_2O_3 \leq 0.005\%$; $Eu_2O_3 \leq 0.0002\%$; $Er_2O_3 \leq 0.0002\%$; $Gd_2O_3 \leq 0.0002\%$; $Tm_2O_3 \leq 0.0002\%$; $Tb_4O_7 \leq 0.0002\%$.

Preparation method of Ni-based alloy + Y_2O_3-deposited metal

The average grain size of mixture powders was 30 μm. After milling, four kinds of pressed compacts were obtained and the thickness was 1 mm. The pressed compacts were preset onto the surface of aluminum after dried at 120 °C, and Ni-based alloy + Y_2O_3/aluminum matrix composite materials could be obtained by laser cladding using continuous wave 3 kW Nd-YAG solid-state laser. Parameters for laser cladding and serial number of specimens were illustrated in Table 2. The overlap ratio was 30%, the scanning speed was 10 mm s^{-1}, and the gas-flow rate is 1.4 L min^{-1}.

Analyzing position and testing methods

Specimens for aluminum matrix composite were obtained by laser cladding of the deposited metals (Ni-based alloys and Y_2O_3) on 6061 aluminum alloy in an argon atmosphere. The specimens were then investigated along the position of cross-section (clad-interface-aluminum substrate) direction and longitudinal direction (1st pass–2nd pass−3rd pass), respectively, as shown in Fig. 1.

The microstructures of the specimens were characterized by means of optical observation, X-ray diffraction (XRD) analysis, and scanning electron microscopy (SEM). A Hitachi S-2700 SEM and Electron Probe Microanalyzer EPMA-8705 equipped with an energy-dispersive spectrometer (EDS) were used for microstructure observations and composition analysis.

The samples for optical and SEM observations were etched in a solution of mixed acid consisted of 1% HF, 1.5% HCl, 2.5% HNO_3, 95% H_2O, and reagent (20%

Table 1 Chemical composition of 6061 Al alloy and Ni-based alloy powder

Materials	Si	Fe	Ni	Cu	Co	Mn	Mg	Cr	Mo	C	Zn	W	Al
6061 Al	0.4–0.8	0.7	–	0.15–0.4	–	0.15	0.8–1.2	0.04–0.35	0.15	–	0.25	–	Bal.
Ni-based alloy	–	6	48	–	8	–	–	14	5	1	–	12	6

Table 2 The numbering and processing parameters of laser-cladding layer

Serial number	Cladding materials	Output power (W)	Scanning speed (mm s^{-1})	Laser-beam shape	Shield gas pressure (inner/outside)	Gas-flow rate (L min^{-1})
1#	Ni-based alloy	1,688	10	Narrow band (diameter: 1 mm)	588/352.8	1.4
2#	Ni-based alloy + 2% Y_2O_3	1,688	10	Narrow band (diameter: 1 mm)	588/352.8	1.4
3#	Ni-based alloy + 6% Y_2O_3	1,688	10	Narrow band (diameter: 1 mm)	588/352.8	1.4
4#	Ni-based alloy + 8% Y_2O_3	1,688	10	Narrow band (diameter: 1 mm)	588/352.8	1.4

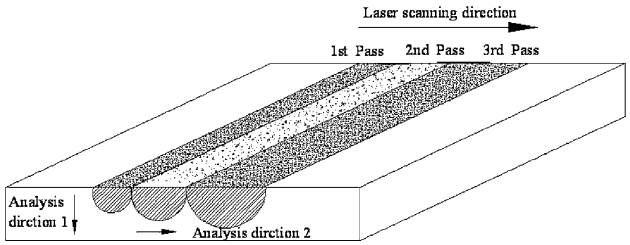

Fig. 1 Illustration for analysis position

KOH + 20% K_3 [Fe $(CN)_6$] + 60% H_2O: vol.%) at room temperature.

Results

The whole morphology distribution of laser clad specimen along cross section direction and laser scanning longitudinal direction is shown in Fig. 2, the macrostructure and microstructure results show that weld bead of deposited metal/aluminum substrate with well-metallurgical bonding is obtained with acicular structure, free from faults such as porosity (air hole), fine hair crack, and slags etc.; SEM image shows that interface reaction has occurred near the fusion line.

Microstructures

Microstructure of 6061 aluminum is illustrated in Fig. 3, from this we can see that the cast structure consists of such phase as Al_2MgCu, $CuAl_2$, α, and Al substrate.

Microstructure of specimen 2# using Ni-based alloy and 2% Y_2O_3 as clad metal on 6061 aluminum substrate was illustrated in Fig. 4a. From the image, we could see that,

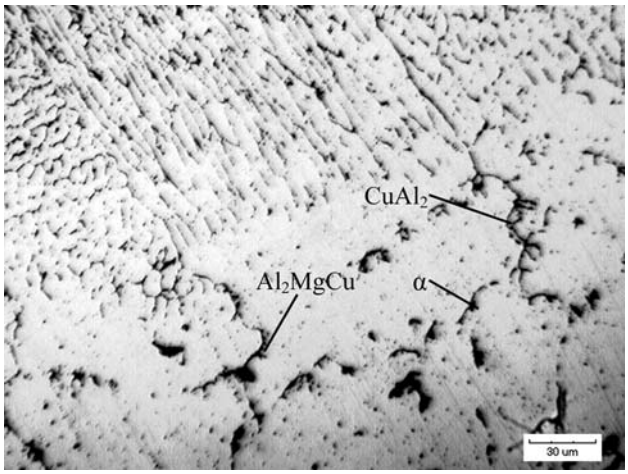

Fig. 3 Microstructure of 6061 aluminum

along the cross section, upper microstructure of deposited metal was consisted of gray isometric crystal, white acicular crystal, and fringe crystal at interface. The average diameter of isometric crystal was 1.6 μm. The microstructure was mainly fine crystal deposited near deposited metals/6061 aluminum substrate interface, a significant transition belt with maximum size of 30 μm was formed. Typical microstructure of deposited metals/6061 aluminum substrate interface near 6061 aluminum side was isometric crystal and arborescent crystal. Some agglomerated particle with finer crystals was formed. The arborescent crystals near interface were opposite to deposited metals/6061 aluminum substrate interface and priority-grown diffusion along this direction. The transition belt was 150 μm at the most. In contrast to different laser scanning passes analysis along longitudinal direction, in the 1st pass, penetration, width, and Heat Affected Zone (HAZ) were smallest. In the

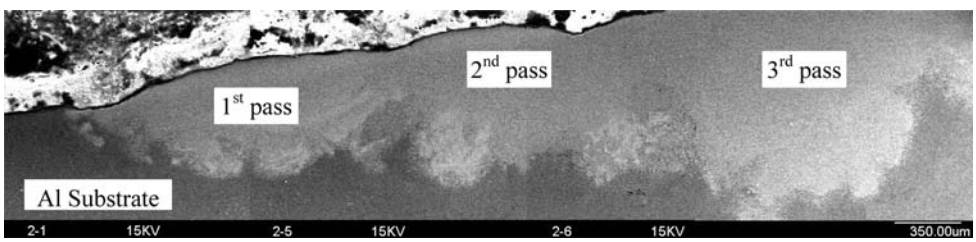

Fig. 2 SEM observation for morphology of three passes laser clad for specimen 2#

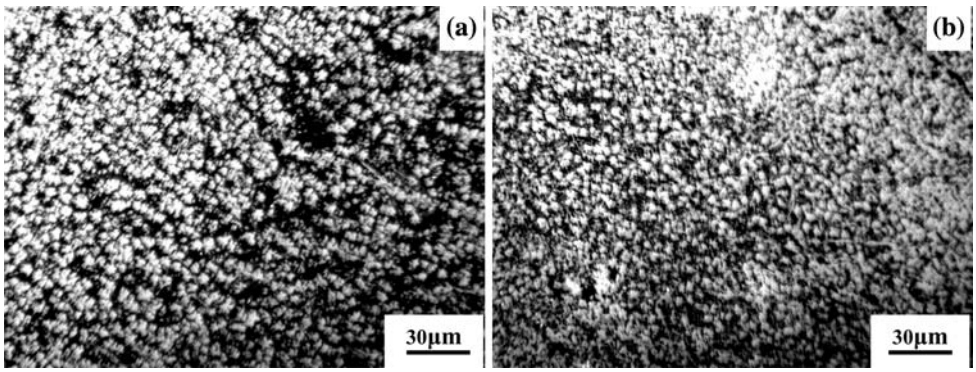

Fig. 4 Microstructure of deposited metal with Ni-based alloy + 2% Y_2O_3 and 8% Y_2O_3. (**a**) Ni-based alloy + 2% Y_2O_3; (**b**) Ni-based alloy + 8% Y_2O_3

2nd pass, width and Heat Affected Zone (HAZ) were smaller, in the 3rd pass, width and HAZ were small with coarse microstructure.

Microstructure of specimen $4^{\#}$ using Ni-based alloy and 8% Y_2O_3 as clad metal on 6061 aluminum substrate was illustrated in Fig. 4b. From the image, we could see, along the cross section, upper microstructure of deposited metal was consisted of more fine gray isometric crystal, white acicular crystal, and fringe crystal at interface than specimen $2^{\#}$. The average diameter of isometric crystal was less than 1 μm. The microstructure was mainly fine crystal under the deposited near-deposited metals/6061 aluminum substrate interface, a significant transition belt with maximum size of 20 μm was formed. Typical microstructure of deposited metals/6061 aluminum substrate interface near 6061 aluminum side was isometric crystal and arborescent crystal. Some agglomerated particle with finer crystals was formed. The arborescent crystals near interface were opposite to deposited metals/6061 aluminum substrate interface and priority-grown diffusion along this direction. The transition belt was 30 μm at the most. The morphology of composite for specimen $4^{\#}$ was illustrated in Fig. 3, from which we could see that, besides above microstructure, acicular crystal, bulk and ellipse reinforced crystals were also formed.

Therefore, for specimen $2^{\#}$ or $4^{\#}$, microstructure distributions abided by aluminum substrate → dendritic crystal + fringe crystal → fine dendritic, disperse reinforced particles and acicular crystal → coarse dendritic crystal.

In contrast to different laser scanning passes analysis along longitudinal direction, in the 1st pass, width and HAZ are smallest. In the 2nd pass, width and HAZ are smaller, in the 3rd pass, width and HAZ are the largest with coarse grain.

SEM observation on specimen $4^{\#}$ is illustrated in Fig. 5. Particulate distribution is shown in Fig. 5a. From the microstructure, we can see that particles manifest uniform size distribution on Ni–Al substrate. Figure 5b illustrates the particulates morphology on Ni–Al zone.

Microstructure of deposited metals/6061 aluminum substrate interface for specimen $2^{\#}$ and specimen $4^{\#}$ is illustrated in Fig. 6; from this we can see that while different cladding materials are chosen, the crystals near deposited metals/6061 aluminum substrate interface manifest different scale, different range, and different morphological characteristics.

SEM observation of typical dendritic crystals near deposited metals/6061 aluminum substrate interface was shown in Fig. 7. Dendritic crystals grew from fusion line and bulk cell coalescence (see Fig. 7a), prior grew along perpendicular to interface. White in black microstructure was formed while cell grew. From the high-resolution SEM image (see Fig. 7b), we could see that there was black bulk microstructure and abscission zone besides dendritic crystals and substrate.

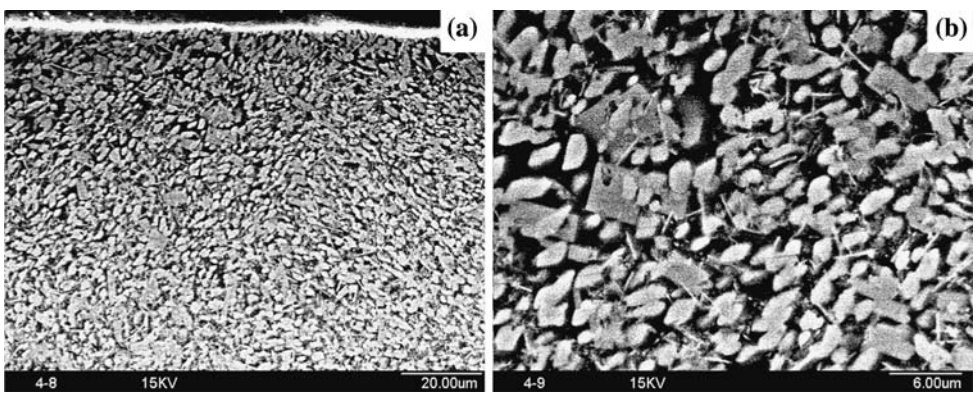

Fig. 5 SEM observation on specimen $4^{\#}$ using Ni-based alloy + 8% Y_2O_3/6061 Al composite as deposited metals. (**a**) Particulates distribution; (**b**) particulates morphology on Ni–Al zone

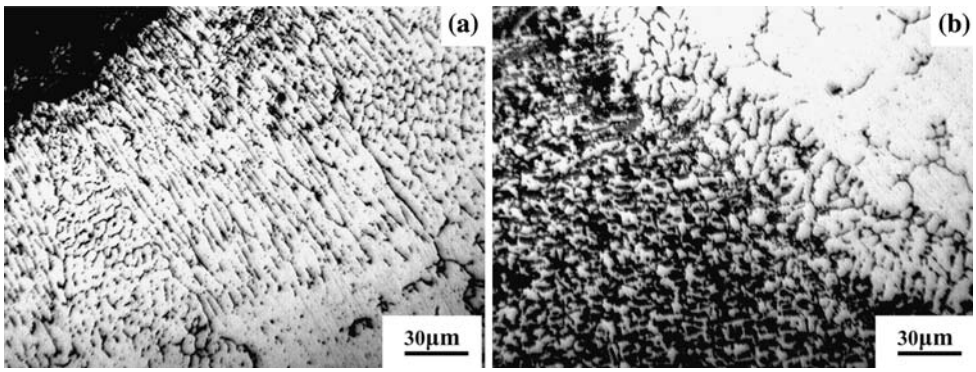

Fig. 6 Microstructure of deposited metals/6061 aluminum substrate interface. (**a**) Specimen $2^{\#}$; (**b**) specimen $4^{\#}$

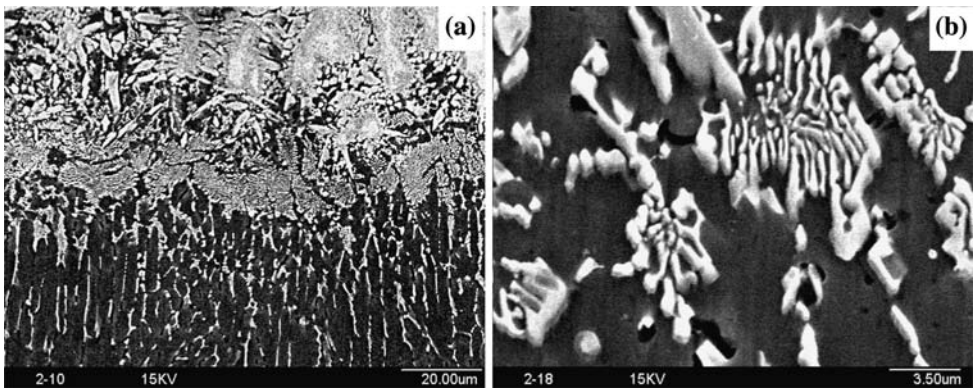

Fig. 7 SEM observation of the Ni-based alloy + 2% Y_2O_3/Al substrate interface, taking the upper side of the interface of the cross section, showing the isometric dendrite crystal and substrate morphology. (**a**) Microstructure distribution at interface; (**b**) several isometric dendrite crystals distribution

Composition and element diffusion

Composition analysis and element diffusion analysis were investigated using EPMA-8705 analyzer. The distribution of elements Ni, Cr, Al, Y, and W near deposited metals/6061 aluminum substrate interface was studied in 500 μm distances between 6061 aluminum substrate and deposited metals. Taking specimen $2^{\#}$ for example, the analysis spectrum 1 and spectrum 2 were illustrated in Fig. 8. The results showed: average composition in white bulk crystal was 57.65% Al, 35.01% Ni, 2.14% Cr, and 1.38% Fe (at.%); average composition in acicular crystal was 64.63% Al, 21.94% Ni, 1.10% Cr, 8.11% Si, and 3.74% Fe (at.%). According to theory calculation, the microstructure might be Ni_xAl, primary phase near deposited metals/6061 aluminum substrate interface was Ni_xAl, Cr_xC was also discovered in this region. Several crystals' compositions and clad matrix for specimen $4^{\#}$ were shown in Table 3.

From the results, white bulk crystal might be Tungsten, and the particles were CrC, which led to dispersion strengthening. Dendritic crystal near deposited metals/6061 aluminum substrate interface was made up of $NiAl_3$, and the clad substrate was NiAl, which led to corrosion resistance.

The distribution of elements Ni, Cr, Al, Y, and W near deposited metals/6061 aluminum substrate interface at 255 and 500 μm distance was investigated for specimen $1^{\#}$, $2^{\#}$, and $4^{\#}$, the results were illustrated in Fig. 9. From the

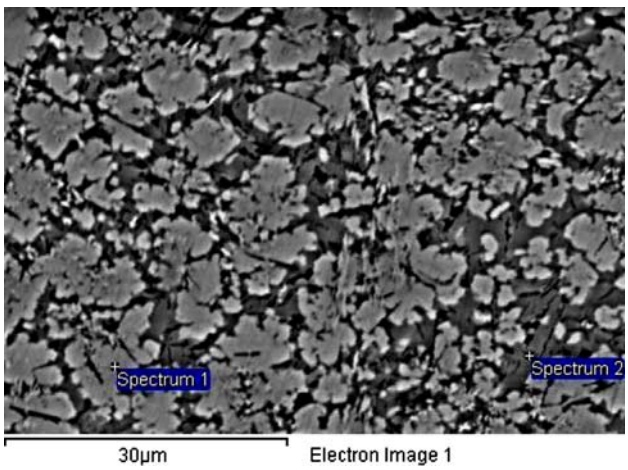

Fig. 8 Composition analysis position of deposited metals/6061 aluminum substrate interface

Table 3 The main compositions of typical microstructure for specimen $4^{\#}$ (at.%)

Typical phase	Ni	Al	Cr	Y	W	C
White bulk crystal	2.11	–	–	–	96.72	1.17
Particles	–	7.17	82.57	–	–	10.26
Dendritic crystal	28.87	69.25	–	1.12	–	0.76
Clad substrate	56.79	42.99	–	0.22	–	–

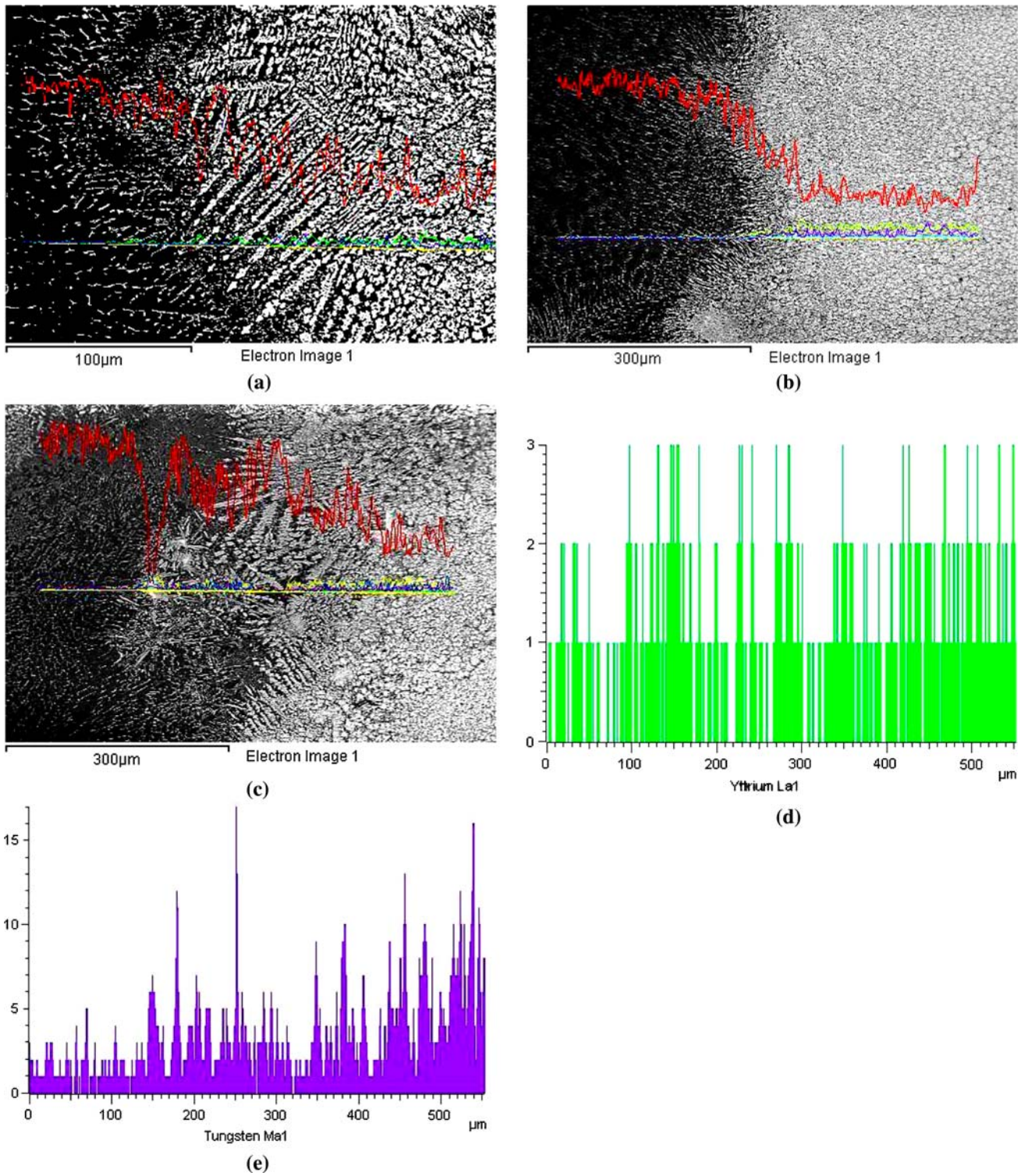

Fig. 9 Line-scanning analysis for element Ni, Cr, Al, Y, and W diffusion near interface in different specimens. (**a**) Line-scanning analysis results for specimen $1^{\#}$ (taking 250 μm near interface red: aluminum; green: nickel; blue: chromium, and no yttrium); (**b**) Line-scanning analysis results for specimen $2^{\#}$ (taking 500 μm near interface, red: aluminum; yellow: nickel; purple: chromium, and cyan: yttrium); (**c**) Specimen $4^{\#}$ (taking 500 μm near interface, red: aluminum; yellow: nickel; blue: chromium; purple: tungsten, and cyan: yttrium); (**d**) Yttrium in specimen $4^{\#}$; (**e**) Tungsten in specimen $4^{\#}$

profiles, in contrast to specimen 1#, gradients of Al, Cr, and Ni are much larger than those of specimen 2# and specimen 4#. Significant Y and W peak could be found in specimen 2# or 4#.

Mechanical properties

Micro-hardness distribution on near deposited metals/6061 aluminum substrate interface of 1#, 2#, 3#, and 4# composites and their corrosion resistance were carried out, respectively.

Micro-hardness test results

After polishing treatment, HXD-1000 type micro-hardness tester was used to investigate the distribution on near deposited metal/6061 aluminum substrate interface, and the results were illustrated in Fig. 10. From the profile, micro-hardness of clad metal (780–1100 $HV_{0.2}$) was much higher than that of aluminum substrate (62 $HV_{0.2}$) significantly.

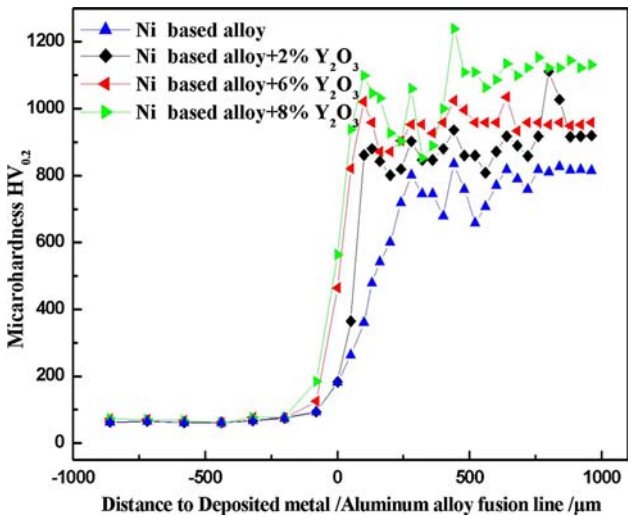

Fig. 10 Micro-hardness distribution on near interface of different composites

In details, for specimen 1#, using Ni-based alloy as deposited metal, much larger width transition zones were achieved from aluminum substrate to deposited metal than those of specimen 2#, 3#, and 4#. This agreed with former microstructure analysis.

Corrosion resistance

The specimen was dried, weighed, and immersed in solution of 10% H_2SO_4 until 4, 8, 12, 16, and 20 h for static corrosion, respectively. After corrosion, specimen was cleaned, dried, and weighed in TG328B analytical balance with 0.1 mg precision. The corrosion was carried out at 50 °C in HH-2 type digital-constant-temperature water bath. The corrosion rate could be calculated by following equation:

$$v_{\text{loss}} = \frac{(m_0 - m_1)}{S \cdot t} \quad (1)$$

where, v_{loss} is corrosion rate; m_0 is mass before corrosion; m_1 is mass after corrosion; S is surface area of specimen; and t is corrosion time.

Corrosion resistance experimental results were illustrated in Table 4. From this we could see that the corrosion rate of aluminum substrate is nearly the double of deposited metal.

After corrosion, the specimen was dried and then analyzed using S-2700 SEM analyzer. The results were shown in Fig. 11. From this we could see that the main corrosion-resistance phase was Ni_xAl, Ni substrate, and remainder Cr_xC reinforced particles, while the aluminum substrate consisted of porous α-Al.

Discussion

According to the above experimental results, the microstructure and mechanical properties change with quantity of addition of Y_2O_3. The details are as follows:

The addition of Y_2O_3 not only improves the weldability of deposited metal on aluminum substrate, but also alters

Table 4 The numbering and processing parameters of laser-cladding layer

Specimen	Mass before corrosion, m_0 (g)	Mass after corrosion, m_1 (g)	Original surface area, S (m^2)	Corrosion time, t (h)	Corrosion rate, v_{loss} (g m^{-2} h^{-1})
Al alloy	0.76685	0.67213	285.4926×10^{-6}	20	16.5889
1#	0.36704	0.35953	45.5479×10^{-6}	20	8.2451
2#	0.02184	0.02145	2.4687×10^{-6}	20	7.8465
3#	0.17032	0.16756	21.1368×10^{-6}	20	6.5248
4#	0.00631	0.00621	0.7831×10^{-6}	20	6.3669

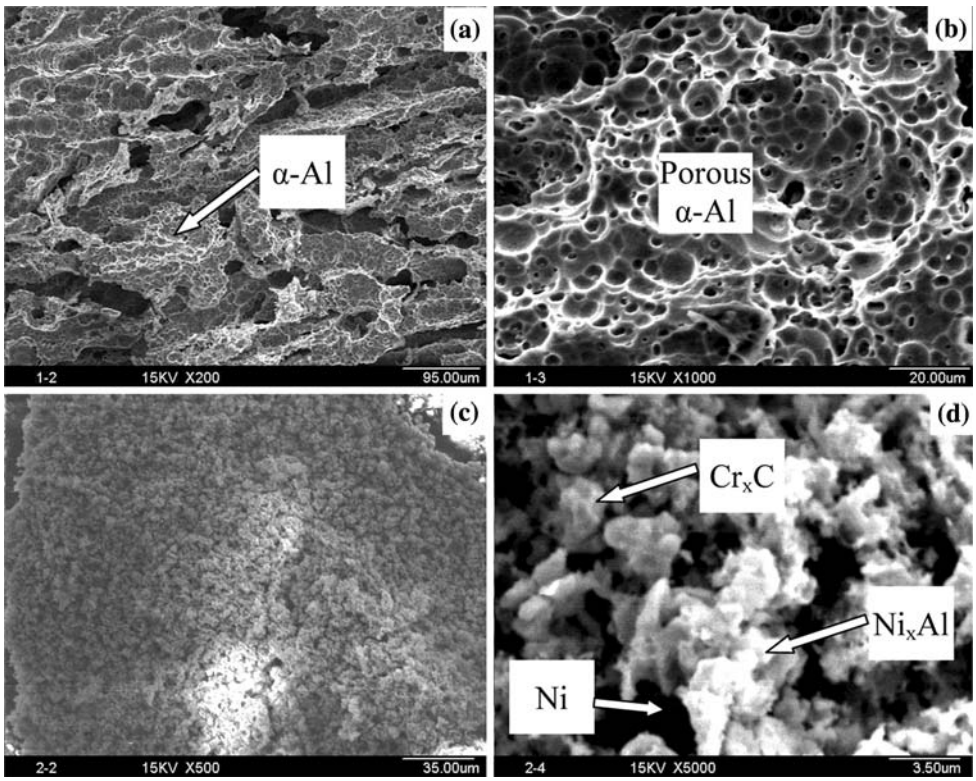

Fig. 11 Corrosion resistance test results of 6061 aluminum substrate and deposited metals in specimen 4#. (**a**, **b**) Morphology of Al substrate after corrosion; (**c**, **d**) morphology of specimen 4# after corrosion

the microstructure and improves the mechanical properties. From Fig. 4, in contrast to 2% Y_2O_3 addition, microstructure of deposited metals with 8% Y_2O_3 manifests more fine crystals; this is because added Y_2O_3 plays a role of grain refinement in microstructure systems.

Contrasting Fig. 6a to b, we can see, that with the increase of Y_2O_3, the crystals near deposited metals/6061 aluminum substrate interface becomes shorter and the transition zone becomes smaller, this agrees with element diffusion analysis results in Fig. 9a–c and micro-hardness distribution test results in Fig. 10.

From the Fig. 10 and Table 4, with increase of Y_2O_3, higher micro-hardness and better corrosion resistance can be obtained. The reason is that fine-crystal strengthening mechanism caused by increase of Y_2O_3 addition plays a significant role in improving the strength. Moreover, Y_2O_3 addition improves the corrosion resistance of Ni_3Al, NiAl, and $NiAl_3$ by decreasing the size of crystal grain and deposited metals/6061 aluminum substrate interface.

Conclusions

(1) The addition of Y_2O_3 improves the weldability of deposited metal on aluminum substrate, alters the microstructure from coarse scales to fine scales, and shortens the transition zone near deposited metals/6061 aluminum substrate interface.

(2) Using laser cladding technique and different cladding materials, well-deposited metal with higher micro-hardness and better corrosion resistance can be obtained. Also with increase of Y_2O_3 addition, the corrosion rate of deposited metal decreases and micro-hardness increases accordingly.

Acknowledgements The authors acknowledge the support of Specialized Research Fund for Excellent Young Teachers of Shanghai, People's Republic of China (Grant No. 06xpyq17), the Scientific Program of Science & Technology Department of Shanghai (Grant No. 061111034), the Youth Foundation of Shanghai University of Engineering Science (Grant No. 06-7), and Specialized funds from Shanghai Municipal Education Commission (No. 06zz79). Many thanks are given to Prof. Shun Yao, Dr. Xinhua Tang, Fenggui Lu, Hailiang Yu, and J. J. Ding from Welding Engineering Institute.

References

1. Qi H, Mazumder J, Ki H (2006) J Appl Phys 100(2):024903
2. Manna I, Dutta Majumdar J, Ramesh Chandra B, Nayak S, Dahotre NB (2006) Surf Coat Technol 201(1–2):434
3. Navas C, Conde A, Cadenas M, De Damborenea J (2006) Surf Eng 22(1):26
4. Li MX, He YZ, Yuan XM, Zhang SH (2006) Mater Design 27(10):1114
5. Xu PQ, Tang XH, Lu FG, Yao S (2006) Sci Technol Weld Joining 11(3):352
6. Xu PQ, Yang D, Zhao XJ, Yao S (2005) J Mater Sci 40(24):6559. doi:10.1007/s10853-005-1547-1
7. Duraiselvam M, Galun R, Siegmann S, Wesling V, Mordike BL (2005) Lasers Eng 15(5–6):355

8. Kadhim MJ, Subhi AD, Moosa AA (2005) 24th International congress on applications of lasers and electro-optics, ICALEO 2005, p 640
9. Xu J, Liu WJ, Kan Y, Zhong ML (2006) Mater Design 27(5):405
10. Xu J, Liu WJ (2006) Wear 260(4–5):486
11. Liu X-B, Wang H-M (2006) Surf Coat Technol 200(14–15):4462
12. Yue TM, Huang KJ, Man HC (2006) Mater Trans 47(3):948
13. Ibrahim IA, Mohamed FA, Lavernia EJ (1991) J Mater Sci 26:1137. doi:10.1007/BF00544448
14. Lloyd DJ (1994) Int Mater Rev 39(1):1
15. Lavernia EJ, Perez RJ, Zhang J (1995) Metall Mater Trans A 26A(11):2803
16. Taya M, Lucay KE (1991) Acta Metall Mater 39(1):73
17. Lebrat JP, Varma A, Miller AE (1992) Metall Trans A 23A(1):69
18. Munir ZA, Umberto AT (1989) Mater Sci R 3(7–8):277
19. Lalas C, Tsirbas K, Salonitis K, Chryssolouris G (2007) Int J Adv Manuf Technol 32(1–2):34
20. Salehi D, Brandt M (2006) Int J Adv Manuf Technol 29(3–4):273